hv photonics

IMPACT FACTOR 1.9

CITESCORE 3.5

Article

Low-Noise Amplification of Coherent Single-Mode Squeezed States

Shaojie Li, Jiachen Liu, Changchang Zhang, Zhaolu Wang, Wenqi Xu, Wenjuan Shi and Hongjun Liu

Special Issue

Quantum Optics: From Fundamental Research to Technological Applications

Edited by

Dr. Georgi Gary Rozenman and Dr. Satyendra Mishra

MDPI

https://doi.org/10.3390/photonics13010051

photonics

MDPI

Article

Low-Noise Amplification of Coherent Single-Mode Squeezed States

Shaojie Li [1,2], Jiachen Liu [1], Changchang Zhang [1], Zhaolu Wang [1,*], Wenqi Xu [1], Wenjuan Shi [1] and Hongjun Liu [1,3,*]

[1] State Key Laboratory of Ultrafast Optical Science and Technology, Xi'an Institute of Optics and Precision Mechanics, Chinese Academy of Sciences, Xi'an 710119, China; lishaojie2023@opt.ac.cn (S.L.); liujiachen1@opt.ac.cn (J.L.); zhangchangchang2017@opt.ac.cn (C.Z.); xuwenqi@opt.ac.cn (W.X.); shiwenjuan@opt.ac.cn (W.S.)
[2] University of Chinese Academy of Sciences, Beijing 100049, China
[3] Collaborative Innovation Center of Extreme Optics, Shanxi University, Taiyuan 030006, China
* Correspondence: wangzhaolu@opt.ac.cn (Z.W.); liuhongjun@opt.ac.cn (H.L.)

Abstract

Quantum noise fundamentally limits the performance of fiber-optic systems beyond the standard quantum limit (SQL), restricting long-distance quantum key distribution, quantum communication, and precision quantum sensing. To overcome these limitations, quantum-squeezed states enable quadrature-dependent noise suppression, yet their benefits rapidly degrade under fiber attenuation, necessitating low-noise amplification. Since conventional phase-insensitive amplifiers (PIAs) impose a minimum 3 dB noise figure (NF) penalty and disrupt quantum correlations, phase-sensitive amplification (PSA) becomes essential. In this work, we propose a PSA based on dual-pump frequency-degenerate four-wave mixing (FWM) to amplify weak coherent squeezed states. Here, the PSA is seeded by an information-carrying single-mode squeezed state, where the information is encoded in the displacement degree of freedom, rather than in the squeezing itself. By optimizing the relative phases among the squeezed state, pump fields, and weak signal, the scheme maintains proper squeezing alignment and preserves the encoded quantum correlations during propagation. Under low-loss conditions, it is shown that the effective NF reaches −7.787 dB, demonstrating that the scheme enables quantum-limited amplification suitable for long-haul transmission and offering a viable path toward scalable fiber-based quantum technologies.

Keywords: quantum squeezed states; four-wave mixing; noise figure; phase-sensitive amplifiers

Received: 1 December 2025
Revised: 24 December 2025
Accepted: 4 January 2026
Published: 6 January 2026

1. Introduction

In recent years, progress in quantum optics has underscored the standard quantum limit (SQL) as a fundamental quantum barrier in contemporary optical systems, persisting as a dominant constraint amid other noise sources [1–11]. In quantum precision metrology, the SQL constrains sensitivities in applications such as magnetometry and interferometry [1], where quantum noise reduces phase sensitivity to the SQL at approximately 60% loss rates [1]. Similarly, in quantum sensing and measurement, particularly in interferometers for gravitational wave detection, SQL restricts precision due to inherent quantum noise such as photon-counting and radiation-pressure errors [3–5], exacerbated by fiber losses and conventional phase-insensitive amplifiers that add at least 3 dB of

noise [6], leading to gain degradation. In quantum communication, SQL-imposed quantum noise fundamentally limits the performance of fiber-optic systems [7], particularly in long-distance and high-capacity scenarios such as quantum key distribution (QKD) [8] and other high-fidelity quantum protocols [9,10]. In these regimes, waveguide losses rapidly diminish the quantum advantages of squeezed states and disrupt the correlations essential for secure long-distance transmission [11]. In particular, in continuous-variable (CV) QKD with homodyne detection, a phase-locked PSA can be placed before Bob's coherent receiver as a low-noise optical pre-amplifier to selectively enhance the information-bearing quadrature, thereby compensating for detector limitations and reducing the input-referred detection noise, which in turn increases the achievable secret key rate [12]. These limitations ultimately highlight the need for advancements in scalable quantum technologies for secure networks and precision sensing.

Squeezed states enable noise squeezing in specific quadratures via nonlinear optics. However, they face two primary challenges in fiber systems: degradation due to losses, which couple to vacuum fluctuations, and disruption of quantum correlations during amplification. Ye et al. optimized gain-loss equilibria in integrated waveguides to sustain squeezing under high-loss regimes, with recent advances enabling arbitrary time-frequency mode squeezing in fiber via self-conjugated modes, achieving up to 7.50 dB [11,13]. Complementing these, Giovannetti and Lloyd's quantum metrology framework demonstrated that coding in lossy channels mitigates noise and underpins anti-attenuation strategies [4], with foundational reviews by Braunstein and van Loock [14] and Paris's quantum estimation theory [15] delineating noise-suppression protocols and parameter bounds in noisy channels. Frascella and colleagues showed that such losses can be mitigated to preserve sub-shot-noise performance at 13% detection efficiency (equivalent to 87% loss) via PSA in second-order parametric systems [3]. To effectively counter these amplification-related disruptions, PSA offers a promising approach by minimizing added noise during signal enhancement. Hansryd, Andrekson, and colleagues demonstrated PSA's superiority over phase-insensitive (PI) counterparts—which incur a 3 dB noise penalty due to quantum limits—whereas fiber-based PSAs, leveraging nonlinear Kerr interferometry, achieve NFs below 3 dB and approaching 0 dB [6]; Tong et al. further validated this in lossy optical links, enabling quantum-noise-limited amplification for long-distance high-fidelity communication [16]. Caves' seminal work established the theoretical basis for PSAs to transcend quantum limits via the amplifier uncertainty principle in optical systems [17]. Collectively, these advances illuminate strategies for generating, transmitting, and amplifying squeezed states in lossy media with minimal noise, with the synergy between squeezed states and PSAs pivotal to preserving quantum correlations against fiber losses and amplifier noise, enabling scalable quantum technologies—such as secure long-haul communication and ultra-precise sensing—to surpass the SQL and advance robust, integrated photonic systems for real-world applications.

PSA of squeezed states enhances weak-signal transmission in optical fibers by countering attenuation and mitigating distortions from quantum noise and losses. By leveraging squeezed-state noise suppression, PSA achieves NFs below classical limits, improving signal fidelity and range. The process first generates a single-mode squeezed state through non-degenerate four-wave mixing (NDFWM) in a self-conjugate scheme [13], followed by amplification using PSA based on dual-pump frequency-degenerate FWM, which in this configuration is implemented as a degenerate four-wave-mixing (DFWM) process, in a polarization-maintaining high-nonlinearity fiber (PM-HNLF). Optimized phase alignment boosts gain while preserving information integrity. This system scheme yields an effective NF as low as −7.87 dB under optimized conditions, enabling quantum-enhanced fiber communications and compact devices.

2. System Design and Theoretical Derivation

2.1. Low-Noise Single-Mode Squeezed States Amplification System Solution

Figures 1 and 2 illustrate the squeezing and amplification sections of a weak-signal low-noise amplification system, respectively, where the former reduces quantum noise and the latter achieves ultra-low-noise amplification.

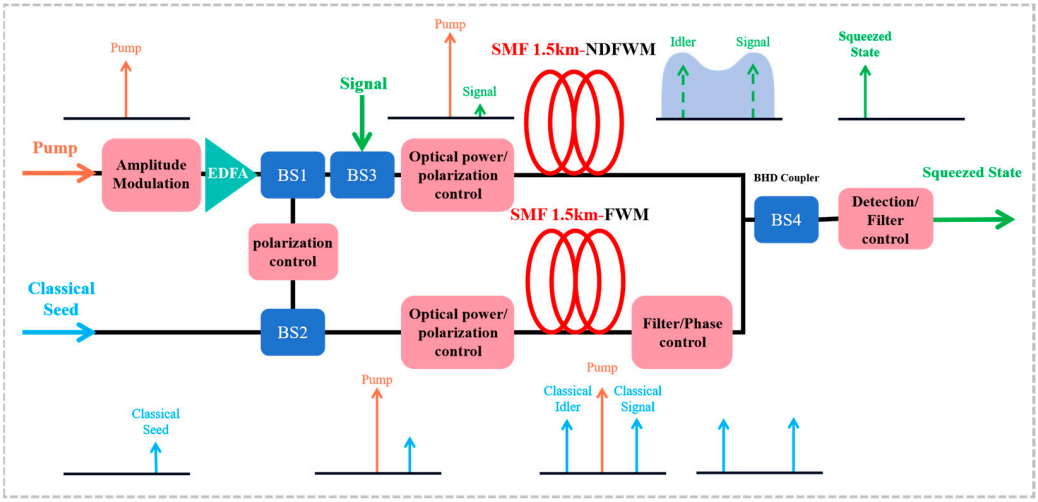

Figure 1. Schematic of the setup for generating information-carrying coherent squeezed states. EDFA: Erbium-Doped Fiber Amplifier; BS1: 50:50 beam splitter; BS2: 10:90 coupler (90% pump port, 10% seed port); BS3: 10:90 coupler (90% pump port, 10% seed port); BS4: 50:50 balanced homodyne detection couple.

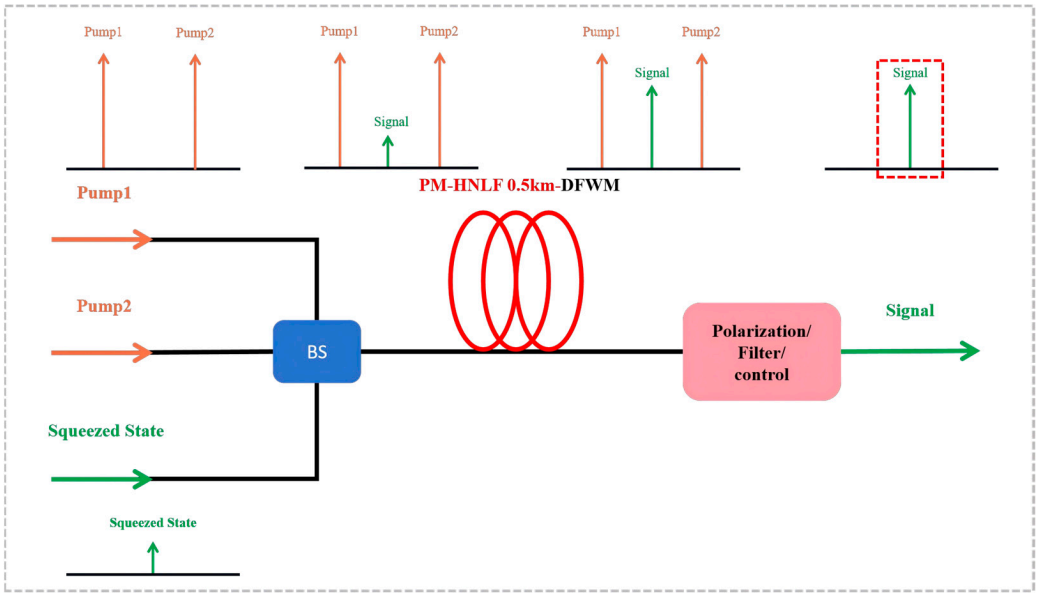

Figure 2. Schematic of the setup for amplifying information-carrying coherent squeezed states. The red dashed box indicates the amplified output of the information-carrying single-mode squeezed state. BS: optical coupler.

The squeezing process illustrated in Figure 1 employs a two-arm configuration, comprising a squeezing arm and a reference arm, to generate coherent single-mode squeezed states that carry encoded information [13]. The signal and idler fields maintain phase-conjugate symmetry throughout the process. The pump beam is generated by modulating a continuous-wave laser into pulses using an electro-optic amplitude modulator (Keyang

Photonics, Beijing, China; Optilab, USA, Phoenix), followed by amplification via an erbium-doped fiber amplifier (EDFA) and filtering with a fiber Bragg grating to suppress amplified spontaneous emission noise. The purified pump is split by a 50:50 coupler into two paths. In the squeezing arm, the pump is routed through a 1.5 km fiber and combined, via a 10:90 coupler (90% pump port, 10% seed port), with an input weak coherent signal at −60 dBm carrying information, generating a coherent squeezed state via NDFWM, where the weak signal approximates vacuum input for theoretical feasibility. The other path enters the reference arm and is combined with classical seed light at −30 dBm via a 10:90 coupler (90% pump port, 10% seed port), yielding classical amplification to produce a balanced self-conjugated (SC)-mode local oscillator (LO) after power tuning with a tunable bandpass filter. The coherent squeezed state from the squeezing arm interferes with the SC-mode LO at a 50:50 balanced homodyne detection coupler, with the output detected by a balanced photodetector. Spectral filters isolate the idler branch for independent homodyne detection as heralding, enabling computation of the signal mode's random displacement from the heralding outcome, followed by compensation through linear interference or data processing. This non-deterministic process yields a coherent single-mode squeezed state that retains the original weak coherent information and demonstrates quantum noise suppression, albeit constrained by the heralding penalty. Overall, this all-fiber design offers low-loss operation and high flexibility [13].

The amplification setup illustrated in Figure 2 uses a high-nonlinear polarization-maintaining fiber (PM-HNLF) with the length of approximately 500 m to amplify the squeezed signal power for transmission. The output from the squeezing section serves as the input, with dual pumps polarization-matched to the signal and phase-adjustable for PSA. The squeezed state and pumps are coupled into the HNLF via an optical coupler, where DFWM, performed under phase-locked conditions between the pumps and the squeezed state, enables efficient amplification by leveraging nonlinear interactions to boost the signal. The output is separated by a polarization beam splitter and filtered with a fiber Bragg grating, yielding an amplified squeezed light field that meets the power requirements essential for long-distance transmission and detection, while preserving information integrity.

2.2. Mechanism of Single-Mode Squeezing in the Lossless Case

SC mode squeezed states are generated via NDFWM [13], producing single-mode squeezed states. Where the pump, signal, and idler fields are represented by quantum operators [18]:

$$\widetilde{E}_p = \sqrt{\hbar\omega}\hat{a}_p, \widetilde{E}_s = \sqrt{\hbar\omega}\hat{a}_s, \widetilde{E}_i = \sqrt{\hbar\omega}\hat{a}_i, \tag{1}$$

here, $\sqrt{\hbar\omega}$ is the normalization factor for field quantization. The left-hand side represents the Fourier amplitude, where the subscripts p, s, and i denote the pump, signal, and idler, respectively. $\hat{a}_s$ and $\hat{a}_s^+$ are the bosonic annihilation and creation operators for the signal field (satisfying $[\hat{a}_s, \hat{a}_s^+] = 1$).

Under the broadband phase-matching approximation with a continuous-wave pump, the SC mode squeezing solution [13] and squeezing parameter r [19] are defined as:

$$U^+CU = \cosh(r)C - \sinh(r)C^+. \tag{2}$$

In Equation (2), C and C^+ are placeholders for the input operators, U and U^+ are process evolution operators and the conjugate form of the evolution operator.

$$r = \frac{1}{2}\gamma|a_p|^2 L, \gamma = \frac{3\omega_p}{8cnA_{eff}}\chi^{(3)}. \tag{3}$$

In Equation (3), the value of the squeezing parameter r reflects the degree of squeezing of the orthogonal components, while L represents the interaction length. The a_p being the normalized complex amplitude (complex envelope) of the pump field such that the instantaneous pump power is $P_p(t) = |a_p(t)|^2$. The nonlinear coefficient γ within the squeezing parameter is defined by the speed of light c in vacuum, the refractive index n, the third-order polarizability $\chi^{(3)}$ of the fiber, and the effective core area A_{eff} of the fiber.

In addition to the squeezing parameter r, the squeezing angle θ_r is introduced to fully specify the spatial squeezing geometry.

$$\theta_r = 2\phi_p + \beta - \pi/2. \tag{4}$$

In Equation (4), this coefficient characterizes the strength of nonlinear effects within the fiber. Here β is the intentional phase difference between the signal phase ϕ_s (which encodes the arbitrary information) and the squeezing angle θ_r of the first squeezing stage. Both ϕ_s and the pump phase ϕ_p used to generate this squeezing angle θ_r are physical quantities determined solely by the initial single-mode squeezing process, allowing β to be continuously tuned to simulate various information-loading and phase-alignment scenarios. The $-\pi/2$ term compensates the intrinsic 90° phase shift from the imaginary unit i in the DFWM Hamiltonian, optimizing alignment for maximum gain and minimum noise in amplification [20].

Next, we calculate the orthogonal quadrature fluctuations of the single-mode squeezed state in the aforementioned SC-mode squeezing scheme:

$$\begin{aligned} C_{out} &= \cosh(r)C_{in} - \sinh(r)C_{in}^+, \\ C_{out}^+ &= \cosh(r)C_{in}^+ - \sinh(r)C_{in}. \end{aligned} \tag{5}$$

So then

$$\begin{aligned} X_1 &= \frac{C_{out} + C_{out}^+}{2} = (\cosh r - \sinh r)\frac{C_{in} + C_{in}^+}{2} = (\cosh r - \sinh r)X_{in}, \\ Y_1 &= -i\frac{C_{out} - C_{out}^+}{2} = (\cosh r + \sinh r)\frac{C_{in} - C_{in}^+}{2} = (\cosh r + \sinh r)Y_{in}, \end{aligned} \tag{6}$$

here, X_1, Y_1 is the operator for the two components of the single-mode squeezed state, and X_{in}, Y_{in} is the operator for the two components of the input weakly coherent state. The resulting orthogonal component variance is [13]:

$$\begin{aligned} \langle \Delta X_1^2 \rangle &= \frac{1}{2}[\cosh r - \sinh r]^2 = \frac{1}{2}e^{-2r}, \\ \langle \Delta Y_1^2 \rangle &= \frac{1}{2}[\cosh r + \sinh r]^2 = \frac{1}{2}e^{2r}. \end{aligned} \tag{7}$$

For weak coherent inputs with information, Poisson noise from displacement redistributes onto quadratures based on orientation between signal phase ϕ_s and squeezed angle θ_r, impacting final fluctuations. The phase difference δ is defined as $\delta = \phi_s - \theta_r/2 + 2m\pi$,

accounting for the quadrature rotation in the Bogoliubov transformation [14]. The quadrature variances are

$$\begin{aligned} \langle \Delta X_1^2 \rangle &= \frac{1}{2}[\cosh r - \cos\delta \sinh r]^2, \\ \langle \Delta Y_1^2 \rangle &= \frac{1}{2}[\cosh r + \cos\delta \sinh r]^2. \end{aligned} \tag{8}$$

2.3. Decomposition of the Amplified Output Field for a Single-Mode Squeezed State in the Lossless Case

Following the generation of the single-mode squeezed state, PSA based on dual-pump frequency-degenerate FWM is employed to increase the signal intensity while preserving the squeezing in the aligned quadrature and maintaining quantum correlations, in contrast to phase-insensitive amplification. The quantum interaction Hamiltonian is given by [21]

$$\hat{H} = \hbar\omega_2 \hat{a}_2^+ \hat{a}_2 + \hbar\omega_{p1} \hat{a}_{p1}^+ \hat{a}_{p1} + \hbar\omega_{p2} \hat{a}_{p2}^+ \hat{a}_{p2} + \hbar v(\kappa \hat{a}_2 \hat{a}_2 \hat{a}_{p1}^+ \hat{a}_{p2}^+ + \kappa^* \hat{a}_2^+ \hat{a}_2^+ \hat{a}_{p1} \hat{a}_{p2}) + H.c., \tag{9}$$

here, $\hat{a}$ and $\hat{a}^+$ denote the bosonic annihilation and creation operators, respectively. The subscript 2 denotes the signal light, whereas the subscripts p_1 and p_2 refer to the two pump beams, κ is the nonlinear coupling coefficient, v is the propagation velocity in the optical medium, and *H.c.* represents Hermitian conjugation. The amplification process employs the single-mode squeezed state from Section 2.1 is SC mode as input. The simplified Equation (2) for the SC mode solution equates to the standard quantum operator form, with C and C^+ as placeholders for input operators, equivalent to the weakly coherent state signal field $\hat{a}_s$ and $\hat{a}_s^+$ input.

From a quantum-information perspective, the interaction Hamiltonian in Equation (9) governs the quadrature-selective transformation of the input quantum state during the amplification process. When the pumps are treated as strong classical fields, Equation (9) reduces to an effective quadratic, phase-sensitive Hamiltonian whose phase defines the amplified and de-amplified quadratures. Consequently, the optimal operating condition in this work is obtained by aligning the Hamiltonian-defined amplified quadrature with the squeezed quadrature of the injected SC-mode state.

Thus, the initial state of signal light $\hat{a}_2$ in the modified Hamiltonian is

$$\begin{aligned} \hat{a}_2(0) &= \nu \hat{a}_s^+(0) + \mu \hat{a}_s(0), \\ \mu &= \cosh(r), \nu = e^{i\theta_r} \sinh(r). \end{aligned} \tag{10}$$

Under the condition of non-depleted pumps [13], the signal field operator satisfies

$$\frac{d\hat{a}_2}{dt} = -\frac{i}{\hbar}[\hat{a}_2, \hat{H}]. \tag{11}$$

As the injected seed power is extremely weak (−60 dBm), and even for a small-signal parametric gain of 25 dB over a 500 m PM-HNLF, the amplified signal remains at the sub-μW level. Here, the value of 25 dB corresponds to dual-pump powers on the order of a few hundred milliwatts (~0.5 W per pump) in typical high-nonlinearity fibers, which means that the pumps operate in a strong continuous-wave fields and can be treated as non-depleted [22].

In DFWM amplification, classical phase matching relies on momentum conservation, enabling efficient energy transfer from the pumps to the signal field. Under nondepleted pumps approximation, the gain is derived from Bogoliubov transformation. The wave-

vector mismatch Δk between pumps and signal, and the gain factor g satisfying the DFWM Hamiltonian in Equation (9) are

$$\begin{aligned} \Delta k &= k_{p1} + k_{p2} - 2k_s, \\ g &= |\kappa| \cdot \left| \sin c\left(\frac{\Delta k L}{2}\right) \right|, \kappa = \frac{2\pi\omega_p}{cn}\chi^{(3)} A_{p1} A_{p2}. \end{aligned} \tag{12}$$

Maximum gain is achieved when $\Delta k = 0$, thereby eliminating destructive interference caused by phase mismatch [22].

Under the condition of classical wave-vector phase matching, substituting the Hamiltonian and neglecting higher-order terms (due to strong pump coherence) yields

$$\frac{d\hat{a}_2}{dt} = -i\kappa_{eff}\hat{a}_2^+(0), \kappa_{eff} = \kappa a_{p1} a_{p2} e^{-i(\varphi_{p1}+\varphi_{p2})}. \tag{13}$$

where φ_{p1} and φ_{p2} are the phases of two pumps. By introducing hyperbolic function integrals into the aforementioned linear differential equation, the solution $\hat{a}_2(L)$ for the amplified signal light after DFWM amplification, with an initial input state of a single-mode squeezed state, is

$$\hat{a}_2(L) = \cosh(gL)\hat{a}_2(0) + ie^{i\varphi}\sinh(gL)\hat{a}_2^+(0), \tag{14}$$

here, φ denotes the phase difference between the pumps and the squeezed state signal. Based on the output field decomposition, optimizing signal-to-noise (SNR) ratio and minimizing noise in amplification requires precise phase alignment, as detailed in subsequent subsections.

3. Results

3.1. Noise Figure, and Gain of Single-Mode Squeezed States in Lossless DFWM Amplification

We first analyze the ideal lossless case to discuss the fundamental noise and gain properties of the squeezed-state-seeded PSA. In this subsection, we derive the NF and gain of a single-mode squeezed coherent state amplified by a lossless dual-pump frequency-degenerate FWM based PSA. Starting from the output field decomposition in Equations (8) and (14), we analyze the influence of the relative phase φ between the PSA pumps and the input squeezed state on the gain G_{PSA}, the phase difference δ on the NF, as well as the effects of compression parameters r and PSA gain G_{PSA} on noise figure and overall gain. As will be shown below, the optimal phase condition directly follows from the structure of the interaction Hamiltonian introduced in Equation (9).

Under this optimal phase condition, the amplified quadrature is aligned with the displacement direction of the input field, such that the encoded information evolves as $\alpha \to G\alpha$ without mixing with vacuum noise, in contrast to phase-insensitive amplification. Accordingly, the mean photon number $N = |\alpha|^2$ is introduced only as a convenient measure of the displacement strength for evaluating the signal-to-noise ratio and noise figure, and does not imply that the input is information-free.

Specifically, the PSA gain G_{PSA} is expressed as

$$G_{PSA} = [\cosh(gL) + \cos\varphi\sinh(gL)]^2. \tag{15}$$

To achieve optimal gain performance in a PSA, the maximum amplification axis must be precisely aligned with the orthogonal component of the injected squeezed coherent state. This optimal condition is satisfied when the relative phase difference $\varphi = 2m\pi$. The

relationship between the phase difference φ and the squeezed angle θ_r of the input state can be derived from the interaction Hamiltonian in Equation (9):

$$\begin{aligned} \hat{H}_{\text{int}} &= \hbar v\left(\kappa \hat{a}_2 \hat{a}_2 \hat{a}_{p1}^{+} \hat{a}_{p2}^{+} + H.c.\right), \\ \hat{a}_{p1} &= a_{p1} e^{i\varphi_{p1}}, \hat{a}_{p2} = a_{p1} e^{i\varphi_{p2}}, \end{aligned} \tag{16}$$

here $\hat{a}_{p1}$, $\hat{a}_{p2}$ and $\hat{a}_s$ are the annihilation operators for the two pump modes and the signal mode, respectively, and κ is the complex nonlinear coupling coefficient.

Treating the pump fields as strong classical fields, we replace the pump operators with $\hat{a}_{p1} = a_{p1} e^{i\varphi_{p1}}, \hat{a}_{p2} = a_{p2} e^{i\varphi_{p2}}$, yielding the effective phase-sensitive Hamiltonian:

$$\hat{H}_{eff} \propto \kappa a_{p1} a_{p2} e^{-i(\varphi_{p1}+\varphi_{p2})} \hat{a}_s^2 + H.c., \tag{17}$$

and the total effective pump phase (multiple definitions: the second-stage amplification process) as

$$\varphi_p = \varphi_{p1} + \varphi_{p2} + \arg(\kappa). \tag{18}$$

The $G_{PSA\text{-}eff}$ is maximum when the quadrature experiencing amplification coincides with the squeezed quadrature of the injected squeezed vacuum state. This optimal alignment requires the phase of the quadratic term in Equation (17) to satisfy

$$\varphi = \varphi_p - \theta_r = \varphi_{p1} + \varphi_{p2} + \arg(\kappa) - \theta_r + 2m\pi, \tag{19}$$

with this standard definition, the condition for optimal gain performance simplifies to $\varphi = 2m\pi$, which directly gives the required phase relationship:

$$\varphi_{p1} + \varphi_{p2} = \theta_r - \arg(\kappa) + 2m\pi. \tag{20}$$

In most experimental configurations where the nonlinear coupling is real and positive ($arg(\kappa) = 0$), this reduces to the particularly simple alignment condition [23]:

$$\varphi_{p1} + \varphi_{p2} = \theta_r + 2m\pi. \tag{21}$$

When the relative phase φ is $(2m+1)\pi$, the $G_{PSA\text{-}eff}$ approaches zero irrespective of the classical wave-vector mismatch Δk. Under optimal phase conditions ($\varphi = 2m\pi$ with the squeezed quadrature perfectly aligned to the signal direction), the output quadrature evolution is derived from Equation (14). Following heralding, the mean displacement of the amplified squeezed quadrature approximately recovers that of the input coherent state [13]. The SNR is evaluated using balanced homodyne detection, which directly measures the mean square $\langle X \rangle^2$ and the variance $\langle \Delta X^2 \rangle$ of the selected quadrature [24]. First, the following expressions represent the mean $\langle X_2 \rangle$ and variance $\langle \Delta X_2^2 \rangle$ of the single-mode squeezed state after amplification:

$$\begin{aligned} \langle X_2 \rangle &= \cosh(gL)\left[\hat{a}_2^{+}(L) + \hat{a}_2(L)\right] + \cos\varphi \sinh(gL)\left[\hat{a}_2(L) + \hat{a}_2^{+}(L)\right] \\ &= \sqrt{2}|\alpha|[\cosh(gL) + \cos\varphi \sinh(gL)], \end{aligned} \tag{22}$$

Then, the variance of the output is

$$\left\langle \Delta X_2^2 \right\rangle = [\cosh(gL) + \cos\varphi \sinh(gL)]^2 \cdot \frac{1}{2}[\cosh r - \cos\delta \sinh r]^2. \tag{23}$$

Thus, the SNR ratio is obtained as

$$SNR_{out} = \frac{4N}{[\cosh r - \cos\delta \sinh r]^2}. \tag{24}$$

The NF measures the additional noise introduced during amplification. Compared to the initial coherent input state, the NF is defined as

$$\begin{aligned} SNR_{in} &= \frac{\left(\sqrt{2}|\alpha|\right)^2}{\frac{1}{2}} = 4N, \\ NF &= \frac{SNR_{in}}{SNR_{out}} = [\cosh r - \cos\delta \sinh r]^2. \end{aligned} \tag{25}$$

Equation (25) clearly shows that NF is minimized when $\delta = 2m\pi$ and degrades rapidly with increasing misalignment due to projection of the strongly anti-squeezed quadrature (variance e^{2r}) onto the measurement axis. At $\delta = (2m+1)\pi$, the squeezing benefit vanishes completely.

The total gain of the light field measures the amplification factor of the field's total energy. We first derive the mean photon number of the single-mode squeezed state. For a single-mode field, the photon number operators $\hat{a}_2$ and $\hat{a}_2^+$ are related to the orthogonal components [25]:

$$\langle n_2(0)\rangle = \langle \hat{a}_2^+(0)\hat{a}_2(0)\rangle = \frac{1}{2}\left(\left\langle \hat{X}_1^2\right\rangle + \left\langle \hat{Y}_1^2\right\rangle - 1\right). \tag{26}$$

Additionally, when the phase difference $\delta = 2m\pi$, the second moment of the two components in the single-mode squeezed state can be expressed as

$$\begin{aligned} \left\langle X_1^2\right\rangle &= \left(\sqrt{2}|\alpha|\right)^2 + \frac{1}{2}[\cosh r - \sinh r]^2, \\ \left\langle Y_1^2\right\rangle &= \frac{1}{2}[\cosh r + \sinh r]^2. \end{aligned} \tag{27}$$

Substituting Equation (27) into Equation (26) gives the photon number for the single-mode squeezed state:

$$\langle n_2(0)\rangle = \frac{1}{2}\left(2N + \frac{1}{2}[\cosh r - \sinh r]^2 + \frac{1}{2}[\cosh r + \sinh r]^2 - 1\right), \tag{28}$$

further simplify this expression to

$$\langle n_2(0)\rangle = N + \sinh^2 r. \tag{29}$$

The total number of photons after amplification is

$$\langle n_2(L)\rangle = \langle \hat{a}_2^+(L)\hat{a}_2(L)\rangle = [\cosh(gL) + \cos\varphi \sinh(gL)]^2 \cdot \left(N + \sinh^2 r\right) + \sinh^2(gL). \tag{30}$$

Thus, the total gain of the light field is obtained as

$$G_{out} = \frac{[\cosh(gL) + \cos\varphi \sinh(gL)]^2 \cdot \left(N + \sinh^2 r\right) + \sinh^2(gL)}{N}. \tag{31}$$

which reaches its maximum value at $\varphi = 2m\pi$ and drops to zero at $\varphi = (2m+1)\pi$, independent of the classical wave-vector mismatch Δk.

Figure 3 shows the *NF* versus phase difference δ for different input squeezing levels (r = 4, 8, and 12 dB) at a fixed parametric gain G_{PSA} of 25 dB (a realistic high-gain value within the range experimentally demonstrated for degenerate FWM-based PSAs [26]). The minimum NF is achieved strictly at $\delta = 2m\pi$, with performance enhanced at higher squeezing levels, confirming Equation (25). Thus, the SNR can be optimized by tuning the squeezing level and enforcing proper phase alignment, while the PSA gain can subsequently be increased to boost the signal without introducing additional noise.

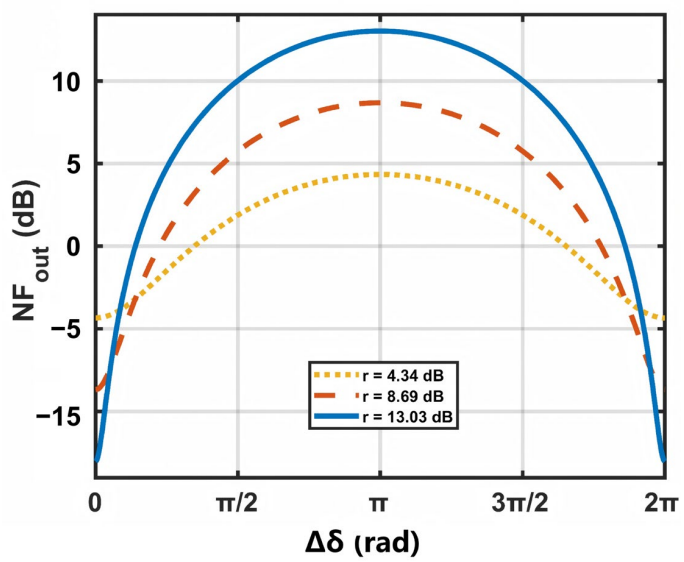

Figure 3. NF as a function of the phase difference δ between the signal phase and the squeezing phase for different input squeezing levels (r = 4, 8, and 12 dB) at a fixed G_{PSA} gain of 25 dB under lossless conditions. The minimum NF is achieved at $\delta = 2m\pi$, with performance degrading symmetrically with increasing phase difference.

Figure 4 presents the output gain G_{out} as a function of phase difference φ for r = 8 dB and several values of Δk. Maximum gain occurs at $\varphi = 2m\pi$ and $\Delta k = 0$, whereas G_{out} approaches its minimum value at $\varphi = (2m + 1)\pi$ irrespective of Δk, conforms to Equation (31).

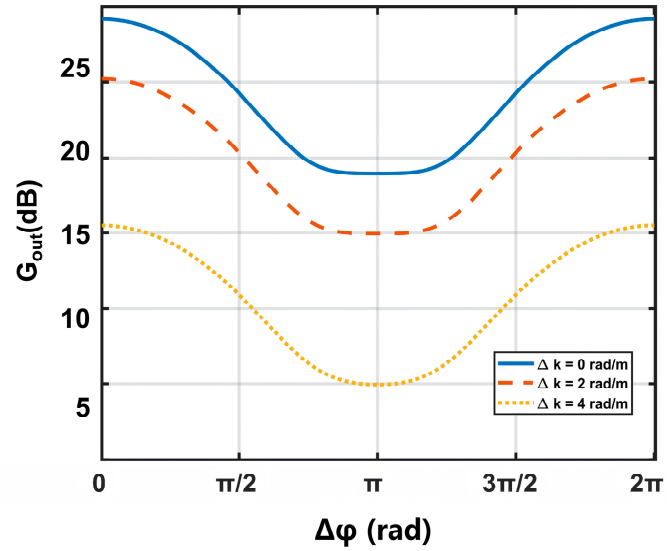

Figure 4. Output gain Gout as a function of the relative phase φ between the pump and the squeezed state under lossy conditions for different classical wave-vector mismatches $\Delta k = 0$, 2, and 4 rad/m. Maximum gain is achieved at $\varphi = 2m\pi$ with $\Delta k = 0$, while the gain profile broadens and decreases with increasing Δk.

To further illustrate the unique advantage of the squeezed-state seeded PSA in the ideal case, Figure 5 presents the output NF and the gain G_{out} as functions of the PSA gain for different input squeezing levels r = 0, 4, 8, and 12 dB under lossless and perfectly phase-matched conditions.

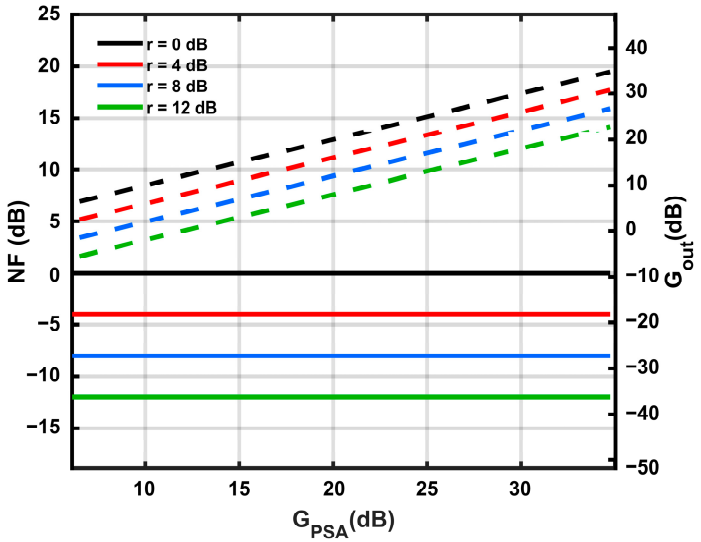

Figure 5. *NF* (solid lines, left axis) and G_{out} (dashed lines, right axis) as a function of the G_{PSA} for different input squeezing levels (r = 0, 4, 8, and 12 dB) in the ideal lossless and perfectly phase-matched case. The NF depends exclusively on the squeezing level r and remains constant irrespective of the G_{PSA}, while arbitrarily high gain can be achieved without degrading the noise performance.

As clearly illustrated in Figure 5, in the ideal lossless and perfectly phase-matched regime, the NF (solid lines, left axis) depends solely on the squeezing parameter r and remains completely independent of the PSA gain G_{PSA}. This occurs because the PSA stage amplifies the already-squeezed quadrature, scaling both signal and (reduced) noise by exactly the same factor, thereby preserving the input squeezing without adding excess noise.

In contrast, the total power gain relative to the original coherent-state seed (dashed lines, right axis) increases exponentially and without limit as G_{PSA} is raised, while NF stays constant. This unique decoupling enables arbitrarily large low-noise amplification simply by increasing the PSA gain once the desired r is achieved—a fundamental advantage over any classical or phase-insensitive amplifier.

In summary, the proposed squeezed-state-seeded degenerate four-wave mixing amplifier effectively combines pre-squeezing and phase-sensitive amplification. Precise control of the relative phase difference φ and δ are essential to approach the quantum limit. In the ideal lossless regime, the NF is determined solely by the input squeezing level r and remains constant irrespective of the PSA gain G_{PSA}, enabling arbitrary low-noise power amplification of the signal. These findings underscore the potential of the scheme for realizing practical ultra-low-noise quantum amplifiers and high-fidelity quantum information processing.

In realistic experiments, distributed fiber loss, inter-stage and output insertion losses, imperfect quantum coupling efficiency, residual phase fluctuations, and background noise cannot be neglected. The following subsection includes these practical imperfections in the model and assesses the achievable performance.

3.2. Single-Mode Squeezing State Under Lossy Conditions via DFWM Amplification Mechanism

3.2.1. Ideal Phase-Matched DFWM Amplification Under Lossy Conditions

Based on the phase sensitivity of δ and φ discussed earlier and the idealized analysis described above, we now extend the model to account for actual loss conditions. To

highlight the fundamental quantum advantage while keeping the treatment tractable, we assume perfect phase difference and phase locking throughout ($\delta = 2m\pi, \varphi = 2m\pi, N \gg 1$), under which the squeezed quadrature variance reduces to e^{-2r}, the anti-squeezed quadrature is fully de-amplified, and the PSA gain along the squeezed axis simplifies to e^{2gL}. Using the effective interaction length $L_{eff} = [1 - exp(2\alpha_f L)]/2\alpha_f$ [11,27], where α_f is the loss coefficient of the fiber, we quantitatively evaluate the impact of input squeezing level r and PSA gain parameter G_{PSA} on the achievable NF and gain, as well as the optimal performance across a wide range of input SNR ratios.

Under loss conditions, the output field evolution incorporates distributed transmission losses through segment efficiencies $\eta_1 = e^{2\alpha_f L_{1-eff}}$ and $\eta_2 = e^{2\alpha_f L_{2-eff}}$ (L_{1-eff} and L_{2-eff} represent the effective lengths of the two fiber segments, respectively). The result is the transmission loss of the two fiber segments, together with the associated vacuum noise contributions ($\langle \hat{\Gamma}_\alpha \hat{\Gamma}_\alpha^+ \rangle = 1$). Under the perfect phase difference condition ($\delta = 2m\pi, \varphi = 2m\pi$) adopted here, these effects modify the single-mode squeezed-state statistics, the expression for the single-mode squeezed state under loss conditions is modified as follows:

$$\hat{a}_{2-loss}(0) = \cosh\left(r_{eff}\right)\hat{a}_s(0) + \sinh\left(r_{eff}\right)\hat{a}_s^+(0), \tag{32}$$

here, r_{eff} represents the effective squeezing parameter influenced by the effective interaction length, defined as

$$r_{eff} = \frac{1}{2}\gamma |a_p|^2 L_{1-eff}. \tag{33}$$

Under loss conditions, the single-mode squeezed state's orthogonal component $\langle X_{1-loss} \rangle$ can be approximated as the input weakly coherent state's orthogonal component $\langle X_{in} \rangle$ [13]. Then, the modified single-mode squeezed state's orthogonal component $\langle X_{1-loss} \rangle$ and variance $\langle \Delta X_{1-loss}^2 \rangle$ of the single-mode squeezed state are expressed as

$$\langle X_{1-loss} \rangle \approx \langle X_{in} \rangle, \langle \Delta X_{1-loss}^2 \rangle = \frac{1}{2} e^{-2r_{eff}}. \tag{34}$$

After accounting for fiber loss during both the generation and amplification stages in the squeezed state, the corrected second-stage output light field $\hat{a}_{2-loss}(L)$ is obtained by adjusting the effective length, transmission efficiency, and vacuum noise effects:

$$\hat{a}_{2-loss}(L) = \cosh(gL_{eff})\hat{a}_{2-loss}(0) + \sinh(gL_{eff})\hat{a}_{2-loss}^+(0). \tag{35}$$

Subsequently, the orthogonal component and orthogonal component variance corrections are further completed, where the expression for the corrected orthogonal component is

$$\langle X_{2-loss} \rangle = e^{gL_{2-eff}} \langle X_{in} \rangle. \tag{36}$$

Accounting for additional insertion loss η_T (primarily from isolators, filters, and coupling between the two fiber segments or at the system output), as well as detector quantum efficiency η_q and residual phase jitter η_{phase}, the final output quadrature mean value $\langle X_{2-total} \rangle$ is

$$\langle X_{2-total} \rangle = \sqrt{\eta_T \eta_q \eta_{phase}^2} e^{gL_{2-eff}} \langle X_{in} \rangle, \tag{37}$$

where typical values of $\eta_T \approx 0.85$, $\eta_q \approx 0.94$, and $\eta_{phase} \approx 0.97$, are readily achievable in experiments [13,28–30].

The corresponding noise variance on the amplified squeezed quadrature is then

$$\langle \Delta X_{2-total}^2 \rangle = \frac{1}{2}\left[\eta_T \eta_q \eta_{phase}^2 e^{2(gL_{eff} - r_{eff})} + (1 - \eta_T \eta_q) + 2N_{env}\right]. \tag{38}$$

The term $(1-\eta_T\eta_q)$ represents vacuum noise introduced by ultimate optical loss and detection loss, while N_{env} accounts for the environmental thermal background (typically satisfying $N_{env} \leq 0.02$ in well-shielded laboratory settings) [31]. This study employs the definition $N_{env} = 0.02$ in simulations.

Under lossy conditions, the SNR expression is derived as follows:

$$SNR_{loss} = \frac{\langle X_{2total}\rangle^2}{\left\langle (\Delta X_{2total})^2 \right\rangle} = \frac{4N\eta_T\eta_q\eta_{phase}^2 e^{2gL_{2-eff}}}{\eta_T\eta_q\eta_{phase}^2 e^{2(gL_{2-eff}-r_{eff})} + (1-\eta_T\eta_q) + 2N_{env}}. \quad (39)$$

The NF expression considering losses is

$$NF_{loss} = \frac{\eta_T\eta_q\eta_{phase}^2 e^{2(gL_{2-eff}-r_{eff})} + (1-\eta_T\eta_q) + 2N_{env}}{\eta_T\eta_q\eta_{phase}^2 e^{2gL_{2-eff}}}. \quad (40)$$

The total gain formula with loss is revised as follows:

$$G_{loss} = \frac{\eta_q\eta_T\eta_{phase}^2 e^{2gL_{2-eff}} N + \eta_q(1-\eta_T) + (1-\eta_q) + N_{env}}{N}, \quad (41)$$

the additional term $\eta_q(1-\eta_T)$ accounts for the vacuum noise from insertion loss that remains coupled via η_q, while $(1-\eta_q)$ represents the irreducible vacuum noise injected by imperfect quantum coupling efficiency at the fiber output (e.g., mode-matching and collection losses).

To demonstrate the performance of the theoretical model under actual experimental conditions ($\eta_T \approx 0.85$, $\eta_q \approx 0.94$, $\eta_{phase} \approx 0.97$, $N_{env} = 0.02$).

Figure 6a shows the NF_{loss} as a function of the PSA gain $G_{PSA\text{-}eff}$ for two representative pre-squeezing levels: r = 0 dB (coherent-state seeding) and r = 8 dB. Compared with the non-squeezed signal, the system performance is improved by 7.85 dB at a squeezing parameter of 8 dB (r_{eff} = 7.936 dB, representing the effective squeezing achievable solely under fiber optic attenuation conditions). This further corroborates that the NF_{loss} derived in Figure 5 under lossless conditions depends solely on the squeezing parameter.

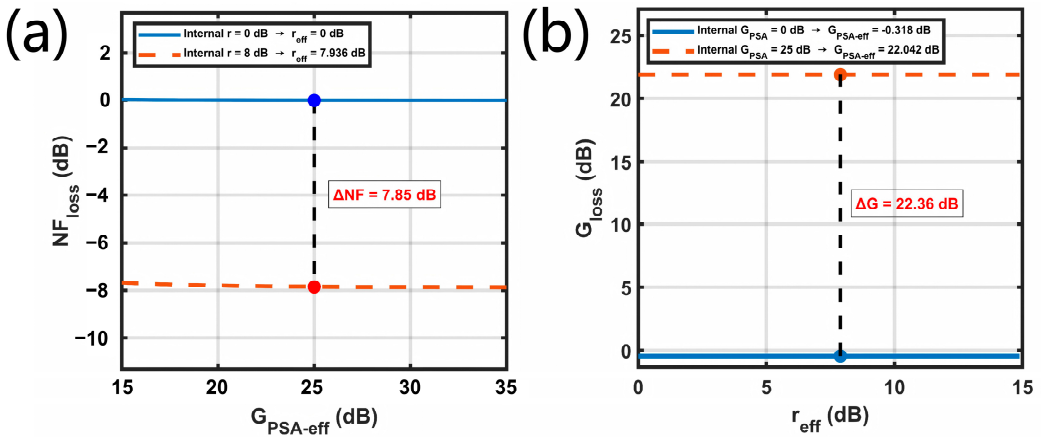

Figure 6. (**a**) NF_{loss} versus PSA gain $G_{PSA\text{-}eff}$ for fixed squeezing levels 0 dB and 8 dB, under realistic losses. (**b**) Total gain G_{loss} vs. pre-squeezing r_{eff} for PSA gain 0 dB and 25 dB under realistic losses.

Figure 6b shows the total power gain G_{loss} as a function of the pre-squeezing parameter r_{eff} for fixed PSA gains G_{PSA} of 0 dB and 25 dB under realistic loss conditions ($G_{PSA\text{-}eff}$ = −0.318 dB and $G_{PSA\text{-}eff}$ = 22.042 dB represent the effective PSA gain under fiber loss conditions only). In typical applications where the input mean photon number satisfies

$|N|^2 \gg 1$, G_{loss} is essentially independent of r_{eff}, confirming that the PSA stage dominates the overall gain, consistent with the lossless analysis in Figure 5. The observed ~3 dB penalty for G_{PSA} = 25 dB originates from the distributed nature of the fiber loss: in the high-gain regime, photons generated early in the fiber are heavily attenuated in the later section, resulting in significantly reduced effective parametric interaction length. The slight upward trend observed for $G_{PSA\text{-}eff}$ = 0 dB arises from residual parametric photons generated in the first stage as r_{eff} increases. Nevertheless, within the currently achievable squeezing range ($r_{eff} \leq 8$ dB), the contribution remains modest, underscoring the necessity of the PSA stage for attaining substantial gain.

To optimize the DFWM squeezed-state amplification system, we define a comprehensive score function that maximizes both squeezing noise suppression and signal gain:

$$Score = 0.5 \times SNR - 0.5 \times NF, \tag{42}$$

Here, the score function is defined as an equally weighted linear combination of SNR_{loss} and NF_{loss}, following the standard weighted-sum method in multi-objective optimization [32], which is use to balance SNR enhancement and NF reduction and to identify a representative Pareto-optimal operating point. The function computes a linear weighted sum of the core parameters SNR_{loss} and NF_{loss} in dB, where absolute values and negative signs are introduced to consistently maximize SNR_{loss} while minimizing NF_{loss}. Combined with boundary conditions from Table 1, Figure 7 analyzes their synergistic effects. By maximizing this optimal evaluation function, the optimization algorithm successfully identifies the synergistically optimal operating point: Combining the constraints in Table 1 [13,33,34], under low-loss conditions, the combination of $r_{eff} \approx 7.838$ dB and $G_{PSA\text{-}eff} \approx 22.192$ dB achieves SNR_{loss} = 13.808 dB (corresponding to a 7.79 dB improvement relative to the input) and G_{loss} = 20.961 dB, $NF_{loss} = -7.787$ dB. This demonstrates that the model can synergistically optimize the squeezing and amplification processes, achieving performance beyond the quantum limit. Equal weights are chosen here for simplicity; alternative weightings would correspond to prioritizing either SNR or NF, depending on the specific application requirements.

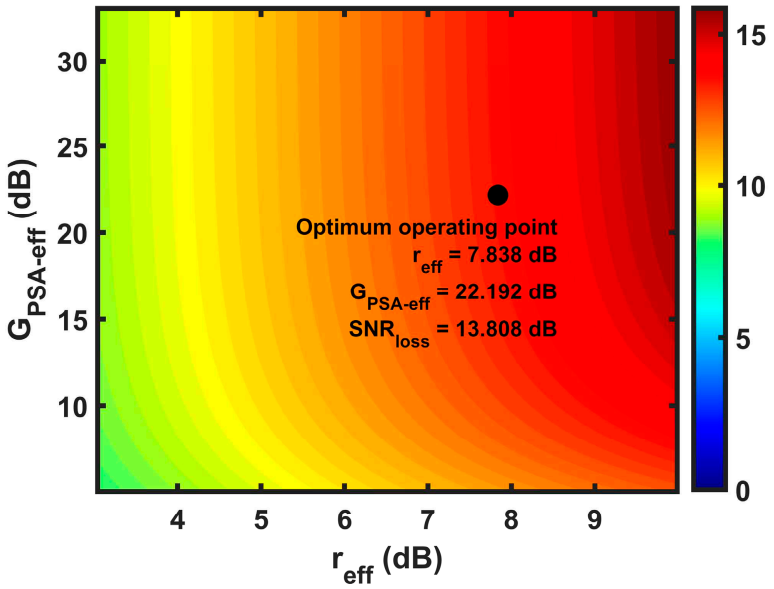

Figure 7. Effect of effective squeezing parameter r_{eff} and PSA gain $G_{PSA\text{-}eff}$ on SNR_{loss} under lossy conditions.

Table 1. Parameters and constraints set in the simulation as above.

Parameters	Constraint Value	Theoretical Basis
PSA Gain $G_{PSA\text{-}eff}$	$\leq$ 25 dB	Balancing high gain levels and nonlinear noise effects in PSA
Squeezing parameters r_{eff}	$\leq$ 8 dB	Loss tolerance limit
Noise Figure NF_{loss}	$\leq$ 3 dB	Classical Amplifier Quantum Limit

Figure 8 demonstrates the robustness of the proposed scheme by plotting the relationship curve between output SNR_{loss} and input SNR_{in} under optimal operating point parameters. Across an input SNR of -5 to 10 dB—from shot-noise-limited weak coherent states to highly noisy signals—the proposed amplifier consistently maintains an NF of approximately -7.78 dB (small ± 0.02 dB fluctuation arising from numerical precision), far superior to an ideal phase-insensitive amplifier.

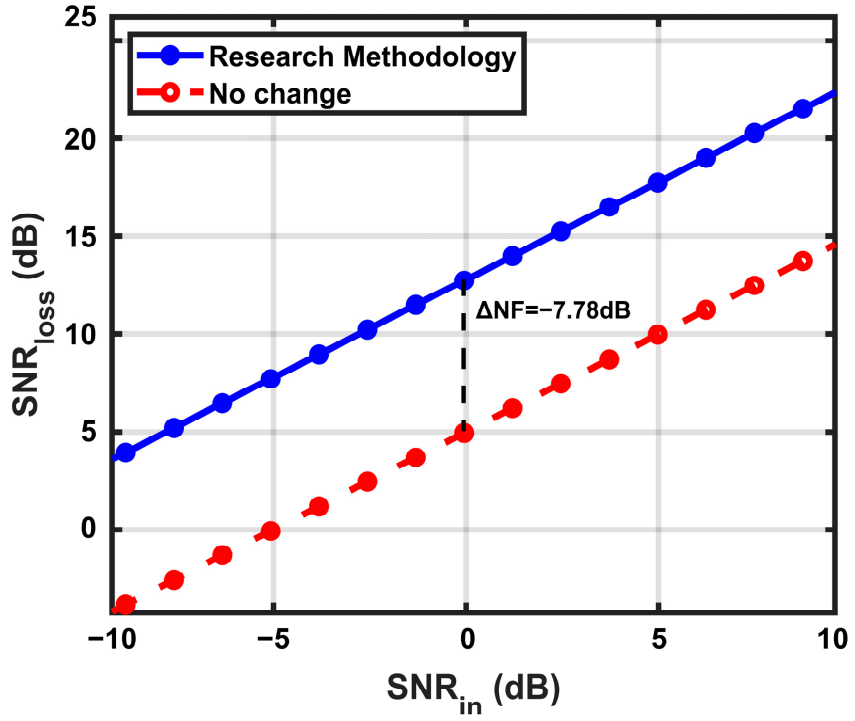

Figure 8. Output SNR_{loss} versus initial input SNR_{in} under lossy conditions (-5 to 10 dB), showing a 7.78 dB improvement in SNR_{out} compared to the reference line ($SNR_{in} = SNR_{out}$).

Overall, we provide a quantitative validation of the proposed theoretical framework, demonstrating that the DFWM-based PSA can simultaneously deliver high gain and a noise figure as low as -7.787 dB under ideal phase matching, while maintaining strong tolerance to realistic non-idealities, including residual phase deviations and variations in the input noise level. This combined performance supports the feasibility of practical quantum-enhanced fiber-optic communication systems and low-noise quantum networks.

3.2.2. Impact of Phase Deviations on Noise Performance

In the above analysis, the optimal operating condition is obtained when the squeezing phase and the pump–signal phase are perfectly aligned, i.e., $\delta = 2m\pi$ and $\varphi = 2m\pi$. In practical fiber systems, however, small phase deviations are unavoidable. In this subsection, we quantitatively evaluate the robustness of the proposed scheme against such phase deviations.

According to Equation (40), under phase-sensitive amplification the NF is fundamentally independent of the PSA gain when amplification is aligned with the information-bearing in-phase quadrature. We discuss a small deviation of the squeezing alignment by writing $\delta = 2m\pi + \Delta\delta$ with $| \Delta\delta | \leq 10^{\circ}$. Under this condition, the effective quadrature variance is given by [35,36]

$$\Delta X^2(\Delta\delta) = V_s \cos^2(\Delta\delta) + V_a \sin^2(\Delta\delta) \tag{43}$$

which follows from the standard covariance-matrix description of a single-mode squeezed state under a rotated measurement quadrature. Here, $V_s = e^{-2r}$ and $V_a = e^{2r}$ denote the squeezed and anti-squeezed quadrature variances, respectively. The corresponding definition of degraded NF is as follows:

$$\Delta NF(\Delta\delta) = \frac{\Delta X^2(\Delta\delta)}{V_s} \tag{44}$$

Figure 9 shows that ΔNF increases rapidly with the squeezing-phase deviation $\Delta\delta$, yielding 1 dB NF degradation with $| \Delta\delta | \approx 4.69^{\circ}$ for 8 dB squeezing and $| \Delta\delta | \approx 1.84^{\circ}$ for 12 dB squeezing [35]. We further consider the impact of the pump–signal phase deviation $\Delta\varphi$ on the G performance. The gain G is given by Equation (41), and the corresponding gain degradation is defined as $\Delta G = |G(\varphi + \Delta\varphi) - G(\varphi)|$. As also shown in Figure 10, the gain degradation exhibits a comparatively weak dependence on $\Delta\varphi$ near the optimal operating point $\varphi = 2m\pi$. It is clear that phase deviations have a significant impact on the robustness of the noise figure NF, while its impact on the robustness of the gain G is relatively minor.

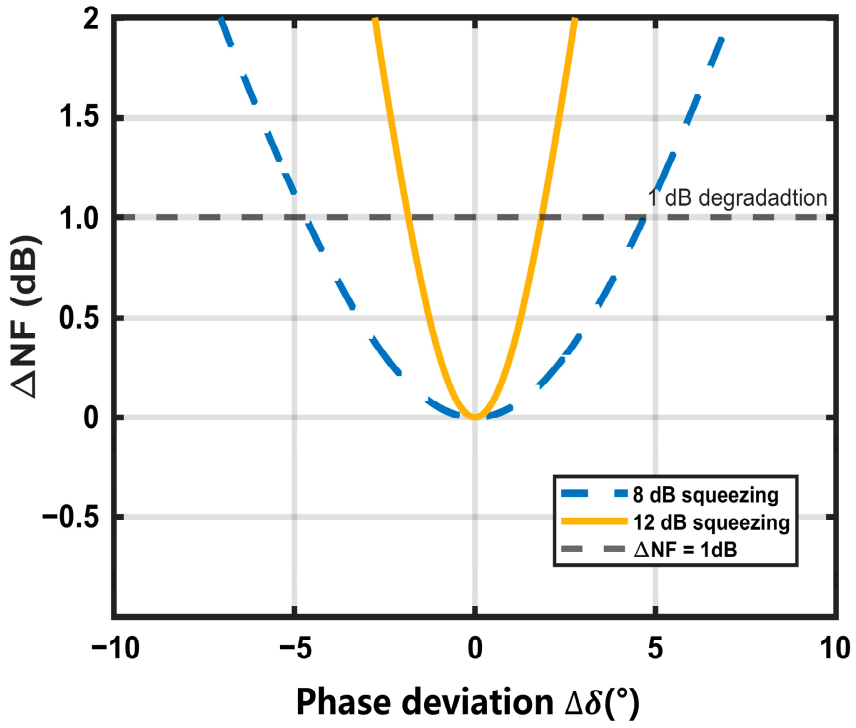

Figure 9. Relative NF degradation ΔNF versus squeezing-phase deviation $\Delta\delta$ for 8 dB and 12 dB squeezing. The horizontal line indicates a 1 dB NF degradation threshold.

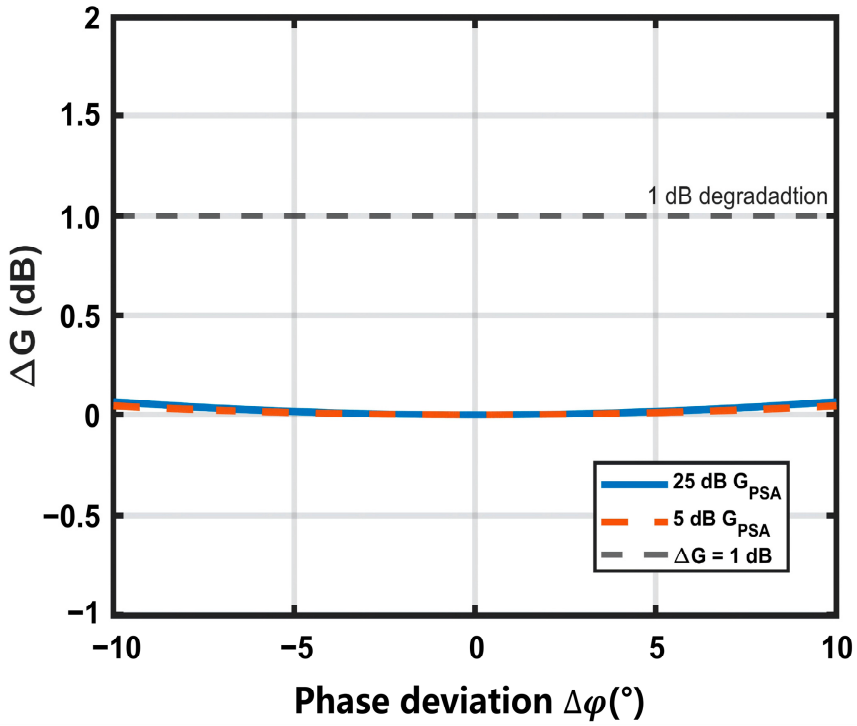

Figure 10. Total gain degradation ΔG versus pump–signal phase deviation $\Delta\varphi$ for $G_{\mathrm{PSA}} = 25$ dB and $G_{\mathrm{PSA}} = 5$ dB. The horizontal line indicates a 1 dB gain degradation threshold.

4. Conclusions

In this work, we show that the squeezing quantum limit impacts the minimum achievable noise figure and the maximum SNR gain in fiber links, thereby determining the ultimate performance of quantum communication in our proposed scheme. In this study, we established a PSA model based on dual-pump frequency-degenerate FWM to enable low noise amplification of weak single-mode squeezed states in fiber. Through studies conducted under both lossless and low-loss conditions, the model elucidates how the phase relationships among the squeezed state, pump fields, and weak signal govern the preservation of quantum correlations during PSA. A central result of this work is that, under optimal phase alignment, the minimum achievable noise figure is fundamentally determined by the effective squeezing parameter and remains independent of the PSA gain. The analysis shows that maintaining phase locking between the dual pumps and the weak squeezed input, together with precise control of the signal pump relative phase, is essential for suppressing excess noise and sustaining stable parametric gain [37]. Under low loss conditions, with effective squeezed parameter r_{eff} = 7.838 dB and effective PSA gain $G_{PSA\text{-}eff}$ = 22.192 dB, the optimal results of $NF_{loss} = -7.787$ dB and G_{loss} = 20.961 dB are obtained. These results confirm that the model supports quantum-limited amplification capable of preserving encoded information over lossy fiber channels. This noise reduction is expected to be particularly beneficial for CV-QKD, where information is encoded in optical field quadratures and retrieved by homodyne detection. In this setting, preserving quadrature squeezing and lowering the effective excess noise enhances the Alice–Bob mutual information I_{AB} while suppressing Eve's accessible information χ_{BE}, thereby extending the secure transmission distance and improving the secret key rate at a given channel loss. These findings provide a practical and scalable foundation for long-distance quantum key distribution, secure quantum communication, distributed quantum sensing, and future classical–quantum hybrid optical networks.

Author Contributions: S.L.: conceptualization, research simulation. J.L.: derivation analysis. C.Z.: formal analysis. Z.W.: conceptualization, derivation analysis, research implementation. W.X.: formal analysis. W.S.: formal analysis. H.L.: formal analysis, conceptualization, funding acquisition. All authors have read and agreed to the published version of the manuscript.

Funding: This research was funded by the National Natural Science Foundation grant number 61975232.

Data Availability Statement: The original contributions presented in this study are included in the article. Further inquiries can be directed to the corresponding authors.

Conflicts of Interest: The author declares no conflicts of interest.

References

1. Heng, X.; Zhang, L.; Yin, Q.; Liu, W.; Tang, L.; Zhai, Y.; Wei, K. Quantum-Enhanced Sensing with Squeezed Light: From Fundamentals to Applications. *Appl. Sci.* **2025**, *15*, 10179. [CrossRef]
2. Huang, W.; Liang, X.; Zhu, B.; Yan, Y.; Yuan, C.-H.; Zhang, W.; Chen, L.Q. Protection of Noise Squeezing in a Quantum Interferometer with Optimal Resource Allocation. *Phys. Rev. Lett.* **2023**, *130*, 073601. [CrossRef]
3. Frascella, G.; Agne, S.; Khalili, F.Y.; Chekhova, M.V. Overcoming Detection Loss and Noise in Squeezing-Based Optical Sensing. *npj Quantum Inf.* **2021**, *7*, 72. [CrossRef]
4. Giovannetti, V.; Lloyd, S.; Maccone, L. Advances in Quantum Metrology. *Nat. Photonics* **2011**, *5*, 222–229. [CrossRef]
5. Caves, C.M. Quantum-Mechanical Noise in an Interferometer. *Phys. Rev. D* **1981**, *23*, 1693–1708. [CrossRef]
6. Andrekson, P.A.; Karlsson, M. Fiber-based phase-sensitive optical amplifiers and their applications. *Adv. Opt. Photonics* **2020**, *12*, 367–428. [CrossRef]
7. Gallion, P.; Mendieta, F.J.; Jiang, S. Signal and quantum noise in optical communications and cryptography. *Prog. Opt.* **2009**, *52*, 149–259.
8. Zhang, Y.; Chen, Z.; Pirandola, S.; Bao, X.; Pan, J. Long-distance continuous-variable quantum key distribution by controlling excess noise. *Sci. Rep.* **2016**, *6*, 19201.
9. Koudia, S.; Chatzinotas, S. Crosstalk-resilient quantum MIMO for scalable quantum communication networks. *npj Quantum Inf.* **2025**, *11*, 162. [CrossRef]
10. Safronova, M.S.; Budker, D.; DeMille, D.; Kimball, D.F.J.; Derevianko, A.; Clark, C.W. Quantum Sensing with Atomic, Molecular, and Optical Platforms for Fundamental Physics. *Phys. Rev. Lett.* **2024**, *132*, 190001. [CrossRef]
11. Ye, Z.; Zhao, P.; Twayana, K.; Karlsson, M.; Torres-Company, V.; Andrekson, P.A. Overcoming the Quantum Limit of Optical Amplification in Monolithic Waveguides. *Sci. Adv.* **2021**, *7*, eabi8150. [CrossRef]
12. Liao, J.; Chen, Z.; Wang, J.; Xiao, H.; Guo, X.; Li, Z.; Wang, D. Experimental demonstration of high-speed continuous variable quantum key distribution enhanced by phase-sensitive amplifier. *npj Quantum Inf.* **2025**, *11*, 105. [CrossRef]
13. Liu, H.; Iu, M.L.; Hamdash, N.; Helmy, A.S. Towards Arbitrary Time–Frequency Mode Squeezing with Self-Conjugated Mode Squeezing in Fiber. *Nat. Commun.* **2025**, *16*, 6524. [CrossRef] [PubMed]
14. Braunstein, S.L.; Van Loock, P. Quantum Information with Continuous Variables. *Rev. Mod. Phys.* **2005**, *77*, 513–577. [CrossRef]
15. Paris, M.G.A. Quantum Estimation for Quantum Technology. *Int. J. Quantum Inf.* **2009**, *7*, 125–137. [CrossRef]
16. Tong, Z.; Lundström, C.; Andrekson, P.A.; McKinstrie, C.J.; Karlsson, M.; Blessing, D.J.; Tipsuwannakul, E.; Puttnam, B.J.; Toda, H.; Grüner-Nielsen, L. Towards Ultrasensitive Optical Links Enabled by Low-Noise Phase-Sensitive Amplifiers. *Nat. Photonics* **2011**, *5*, 430–436. [CrossRef]
17. Caves, C.M. Quantum Limits on Noise in Linear Amplifiers. *Phys. Rev. D* **1982**, *26*, 1817–1839. [CrossRef]
18. Marhic, M.E.; Hsia, C.-H. Optical Amplification and Squeezed-Light Generation in Fibre Interferometers Performing Degenerate Four-Wave Mixing. *Quantum Opt.* **1991**, *3*, 341. [CrossRef]
19. Voss, P.L.; Köprülü, K.G.; Kumar, P. Raman-Noise-Induced Quantum Limits for $\chi^{(3)}$ Nondegenerate Phase-Sensitive Amplification and Quadrature Squeezing. *J. Opt. Soc. Am. B* **2006**, *23*, 598–610. [CrossRef]
20. McKinstrie, C.J.; Raymer, M.G.; Radic, S.; Vasilyev, M.V. Quantum mechanics of phase-sensitive amplification in a fiber. *Opt. Commun.* **2006**, *257*, 146–163. [CrossRef]
21. Seifoory, H.; Vernon, Z.; Mahler, D.H.; Menotti, M.; Zhang, Y.; Sipe, J.E. Degenerate Squeezing in a Dual-Pumped Integrated Microresonator: Parasitic Processes and Their Suppression. *Phys. Rev. A* **2022**, *105*, 033524. [CrossRef]
22. Agrawal, G.P. *Nonlinear Fiber Optics*, 6th ed.; Chapter 10.3; Academic Press: Cambridge, MA, USA, 2009.
23. Zhang, J.; Ye, C.; Gao, F.; Xiao, M. Phase-Sensitive Manipulations of a Squeezed Vacuum Field in an Optical Parametric Amplifier inside an Optical Cavity. *Phys. Rev. Lett.* **2008**, *101*, 233602. [CrossRef] [PubMed]
24. Xiao, M.; Wu, L.-A.; Kimble, H.J. Detection of amplitude modulation with squeezed light for sensitivity beyond the shot-noise limit. *Opt. Lett.* **1988**, *13*, 476–478. [CrossRef]

25. Walls, D.F.; Milburn, G.J. *Quantum Optics*, 2nd ed.; Chapter 5, Squeezed States; Springer: Berlin/Heidelberg, Germany, 2008.
26. Weerasuriya, R.U.; Chen, J.; Larsson, R.; Andrekson, P.A. Pump Frequency Allocation and Dispersion Effect on Dual-Pump Phase Sensitive Amplifier Gain Spectrum. *IEEE Photonics Technol. Lett.* **2025**, *37*, 1273–1276. [CrossRef]
27. Yoshida, M.; Kasamatsu, T.; Okamoto, S.; Ono, T.; Mizuno, T.; Miyamoto, Y. Theoretical and Experimental Analyses of GAWBS Phase Noise in Multi-Span Optical Fiber Transmission Systems. *Opt. Express* **2020**, *28*, 2873.
28. Yang, P.-F.; Zhang, P.-F.; Li, G.; Zhang, T.-C.; Zou, C.-L. Self-Induced Optical Non-Reciprocity. *Light Sci. Appl.* **2024**, *13*, 285.
29. D'Angelo, M.; Peotta, S.; Barbieri, M.; Paris, M.G.A. Quantum Enhanced Non-Interferometric Quantitative Phase Imaging. *Light Sci. Appl.* **2023**, *12*, 181.
30. Huang, T.; Xu, M.; Jin, W.; Liu, W.; Chi, Y.; Tang, J.; Ren, P.; Wei, S.; Bai, Z.; Shi, Y. On-Chip Quantum Interference of Indistinguishable Single Photons from Integrated Independent Molecules. *Nat. Nanotechnol.* **2025**, *20*, 1748–1756. [CrossRef]
31. Pankratov, A.L.; Revin, L.S.; Gordeeva, A.V.; Yablokov, A.A.; Kuzmin, L.S.; Il'Ichev, E. Towards a Microwave Single-Photon Counter for Searching Axions. *npj Quantum Inf.* **2022**, *8*, 61. [CrossRef]
32. Kim, I.Y.; de Weck, O.L. Adaptive Weighted Sum Method for Multiobjective Optimization: A New Method for Pareto Front Generation. *Struct. Multidiscip. Optim.* **2006**, *31*, 105–116. [CrossRef]
33. Gao, M.; Kurosu, T.; Inoue, T.; Namiki, S. Efficient Phase Regeneration of DPSK Signal by Sideband-Assisted Dual-Pump Phase-Sensitive Amplifier. *Electron. Lett.* **2013**, *49*, 140–141. [CrossRef]
34. Kashiwazaki, T.; Yamashima, T.; Enbutsu, K.; Kazama, T.; Inoue, A.; Fukui, K.; Endo, M.; Umeki, T.; Furusawa, A. Over-8-dB Squeezed Light Generation by a Broadband Waveguide Optical Parametric Amplifier toward Fault-Tolerant Ultra-Fast Quantum Computers. *Appl. Phys. Lett.* **2023**, *122*, 234003. [CrossRef]
35. Dwyer, S.; Barsotti, L.; Chua, S.S.Y.; Evans, M.; Factourovich, M.; Gustafson, D.; Isogai, T.; Kawabe, K.; Khalaidovski, A.; Lam, P.K.; et al. Squeezed Quadrature Fluctuations in a Gravitational Wave Detector Using Squeezed Light. *Opt. Express* **2013**, *21*, 19047–19060. [CrossRef] [PubMed]
36. Takeno, Y.; Yukawa, M.; Yonezawa, H.; Furusawa, A. Observation of −9 dB quadrature squeezing with improvement of phase stability in homodyne measurement. *Opt. Express* **2007**, *15*, 4321–4327. [CrossRef]
37. Usenko, V.C.; Grosshans, F. Unidimensional Continuous-Variable Quantum Key Distribution. *Phys. Rev. A* **2015**, *92*, 062337. [CrossRef]